Geophysical Journal International

Geophys. J. Int. (2017) **209,** 1389–1397
Advance Access publication 2017 March 8
GJI Geomagnetism, rock magnetism and palaeomagnetism

doi: 10.1093/gji/ggx098

Cobb Mountain Subchron recorded at IODP Site U1306 (Eirik Drift, off SE Greenland)

J.E.T. Channell

Department of Geological Sciences, University of Florida, P.O. Box 112120, *Gainesville, FL* 32611, *USA. E mail: jetc@ufl.edu*

Accepted 2017 March 7. Received 2017 March 3; in original form 2016 November 1

SUMMARY

The Cobb Mountain Subchron (CMS) is recorded over ∼5 m of core at ∼180 metres composite depth in the sediment sequence recovered at IODP Site U1306, in an interval where sedimentation rates are estimated at ∼15 cm kyr^{-1}. The relatively high-resolution record of the CMS was acquired from u-channel samples from multiple core sections from four holes drilled at the site. Large-scale swings in magnetization directions at the onset of the subchron lead to virtual geomagnetic poles (VGPs) looping over the Indian Ocean, followed by a looping transit northward through the central Pacific Ocean, a ∼10 kyr (∼1.7 m) interval of VGPs at high northern latitudes particularly in the North Atlantic and NW Pacific Oceans, followed by an abrupt normal to reverse transition as VGPs track southward through Africa. Although the VGP paths are intricate and complex, they can be compared with other CMS VGP paths from Pacific and Atlantic sites, including ODP Sites 983 and 984. The age model for Site U1306 places the CMS in the 1178–1215 ka interval (∼37 kyr duration) which bridges marine isotope stages 35–36.

Key words: Palaeointensity; Rapid time variations; Reversals: process, time scale, magnetostratigraphy.

1 INTRODUCTION

The Cobb Mountain Subchron (CMS) is a brief (∼37 kyr) normal polarity subchron at ∼1.2 Ma, just prior to the Jaramillo Subchron, that has been recorded over a large portion the globe, in the Atlantic oceans, in the eastern and western Pacific Ocean, and off Antarctica (references below). These studies have established the existence of the subchron and contributed to its age, but have usually not looked in detail at the field structure associated with the subchron, either because the records had low resolution (low sedimentation rate) or poor fidelity. On the other hand, Clement (1992, 2000) and Yang *et al*. (2001) argued that similarity of virtual geomagnetic pole (VGP) paths for the CMS from the North Atlantic and western Pacific Oceans indicate large scale, or dipolar, symmetries in the CMS transition field.

The CMS takes its name from Cobb Mountain, California (CA), where the Alder Creek rhyolite yielded normal polarity magnetizations within the mainly reversed polarity Matuyama Chron (Mankinen *et al.* 1978). Subsequently, Mankinen & Grommé (1982) found a normal polarity zone in lavas of approximately the same age in the Coso Range (CA). The Alder Creek rhyolite at Cobb Mountain has ^{40}Ar/^{39}Ar ages (Turrin *et al.* 1994; Nomade *et al.* 2005) of 1201 ± 2 ka, when adjusted for the Fish Canyon sanidine standard age of 28.201 Ma advocated by Kuiper *et al*. (2008). Singer (2014) reported new ages for the Alder Creek rhyolite with a weighted mean of 1189 ± 2 ka and considered this age to be appropriate for the end of the CMS. Singer (2014) adopted an age of 1221 ± 11 ka for the onset of the CMS based on ^{40}Ar/^{39}Ar ages of normally magnetized basaltic lavas in the East Carpathians (Panaiotu *et al.* 2013).

The first recognition of the CMS in (marine) sediments was from North Atlantic Deep Sea Drilling Project (DSDP) Site 609 and Ocean Drilling Program (ODP) Site 647 (Clement & Kent 1987; Clement & Martinson 1992), with its occurrence at Site 609 correlating with marine isotope stages (MIS) 35–37 (Ruddiman *et al.* 1989). By correlation of the δ^{18}O records from ODP Site 677 to DSDP Site 607, where the CMS was recorded (Ruddiman *et al.* 1989), Shackleton *et al*. (1990) correlated the CMS to the base of MIS 35 and assigned an age of 1.19 Ma.

Apart from the sites mentioned above, the CMS has been recorded in sediments in the Celebes and Sulu Seas (Hsu *et al.* 1990), in the Lau Basin (Abrahamsen & Sager 1994), off the California Margin (Hayashida *et al*. 1999; Guyodo *et al.* 1999), in the western Philippine Sea (Horng *et al*. 2002, 2003), in the West Caroline Basin (Yamazaki & Oda 2005), off the Antarctic Peninsula (Guyodo *et al.* 2001) and on Bermuda Rise (Yang *et al.* 2001). North Atlantic occurrences include ODP Site 980 (Channell & Raymo 2003), ODP Site 982 (Channell & Guyodo 2004) and Integrated Ocean Drilling Program (IODP) Sites U1304 (Xuan *et al.* 2016) and U1308 (Channell *et al*. 2008, 2016).

At ODP Site 1063 (Bermuda Rise), the CMS is manifested over ∼3.4 m of core (Yang *et al.* 2001), however, oxygen isotope data

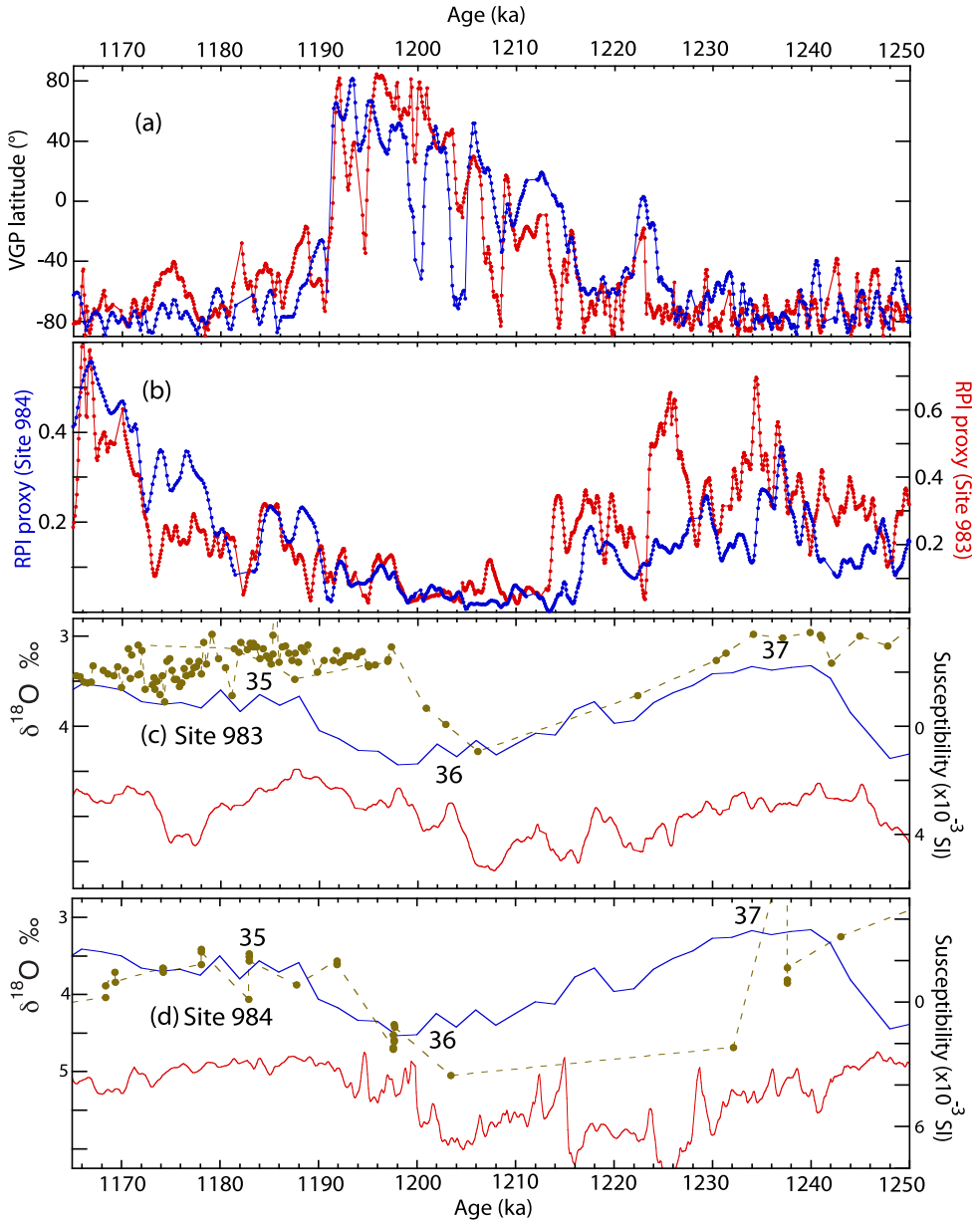

Figure 1. Cobb Mountain Subchron: (a) virtual geomagnetic pole (VGP) latitudes for ODP Site 983 (red) and Site 984 (blue). (b) Relative palaeointensity (RPI) proxies for ODP Site 983 (red) and Site 984 (blue). (c) Site 983: volume magnetic susceptibility (red), benthic oxygen isotope data (brown dots joined by dashed line) and the LR04 oxygen isotope template (blue) of Lisiecki & Raymo (2005) with marine isotope stages 35–37 labeled. (d) Site 984: volume magnetic susceptibility (red), benthic oxygen isotope data (brown dots joined by dashed line) and the LR04 oxygen isotope template (blue) of Lisiecki & Raymo (2005) with marine isotope stages 35–37 labeled (data and age model from Channell *et al.* 2002).

are not available in the relevant interval at this site. At ODP Sites 983 and 984 (Iceland Basin), the CMS is manifested over 2–3 m of stratigraphic section (Channell *et al.* 2002), as opposed to ∼1–1.5 m at DSDP Site 609 and IODP Site U1308. The oxygen isotope data in the vicinity of the CMS at ODP Sites 983/984 were derived from the benthic foraminifera *Cibicidoides wuellerstorfi* and *C. kullenbergi* although foraminifera are only sporadically present in the CMS interval (Raymo *et al.* 1998). To derive the age models in the CMS interval at Sites 983/984, Channell *et al*. (2002) matched the sparse benthic oxygen isotope data to the calibrated δ^{18}O reference record from ODP Site 677 (Shackleton *et al.* 1990), and used the Site 983/984 magnetic susceptibility records to facilitate correlation to the reference δ^{18}O record. In Fig. 1, the δ^{18}O and susceptibility records from Sites 983/984, placed on the age model of Channell *et al*. (2002), are compared with the LR04 (Lisiecki & Raymo 2005) δ^{18}O reference template. Based on comparison with LR04, the age of the CMS at Sites 983/984 should probably be modified from 1190 to 1220 ka (Channell *et al.* 2002) to 1180–1210 ka (Fig. 1).

The record of the CMS at Site U1306 is observed over ∼5 m of core, and is therefore, based on sedimentation rate, the highest resolution record of the CMS currently available.

2 IODP SITE U1306

IODP Site U1306 (58.23°N, 45.64°W) was occupied during IODP Expedition 303 and is located on Eirik Drift (off SW Greenland) at a water depth of 2272 m. The dominant Quaternary lithology

at the site is silty clay with mean sedimentation rates of ∼15 cm kyr^{-1} (Expedition 303 Scientists 2006). Four holes at the site were used to derive an optimal composite section or sampling splice (Expedition 303 Scientists 2006). Although the composite section extends to 337 metres composite depth (mcd), post-cruise u-channel magnetic measurements only involved the upper 215 mcd (Channell *et al.* 2014) because, below this depth, u-channel sampling was impractical due to sediment compaction. Magnetic data from the u-channel sampling of the composite section, and planktic δ^{18}O data from the same composite splice, demonstrate a well-defined magnetic polarity stratigraphy back to 1.5 Ma with δ^{18}O data extending back to 1 Ma (Channell *et al.* 2014). For magnetic and physical properties of Site U1306 Quaternary sediments, see Expedition 303 Scientists (2006), Kawamura *et al*. (2012) and Channell *et al*. (2014).

The CMS is well defined in the composite section at Site U1306 (Channell *et al.* 2014). Here, we compare component magnetization directions and relative palaeointensity (RPI) data from multiple Site U1306 core sections in the CMS interval. We were permitted to sample holes outside the composite section in order to better establish magnetization directions and RPI across the CMS.

3 METHODS

U-channel samples (2 cm × 2 cm × 150 cm 'continuous' samples encased in a plastic liner) were collected from all available Site U1306 core sections recording the CMS, other than core sections within the designated permanent archive. Magnetic methods follow those used for the composite section at this site (Channell *et al.* 2014). All u-channel measurements were carried out at 1 cm intervals with a 10 cm leader and trailer for measurement of u-channel end-effects. Note that adjacent 1 cm measurements are not independent due to the ∼4.5 cm width at half-height of the magnetometer response function (Weeks *et al.* 1993; Guyodo *et al.* 2002). After initial measurement of natural remanent magnetization (NRM), each u-channel sample was subjected to alternating field (AF) demagnetization in 5 mT steps in the 10–50 mT peak field range and in 10 mT steps in the 50–100 mT range. After NRM measurement, anhysteretic remanent magnetization (ARM) was imposed along the long axis of the u-channel sample in a 100 mT alternating field and a 50 μT direct current bias field. The ARM was then demagnetized in the same peak field increments used for NRM, and measured after each demagnetization step. Other magnetic measurements carried out at Site U1306 include volume susceptibility, ARM acquisition, AF demagnetization of isothermal remanent magnetization, hysteresis ratios and first-order reversal curves (Channell *et al.* 2014).

Component magnetization directions were determined using standard methods (Kirschvink 1980) for a uniform 20–80 mT demagnetization interval using the software of Xuan & Channell (2009). Maximum angular deviation (MAD) values provide a measure of the quality of the component directions. RPI proxies were determined as the slopes of NRM demagnetization versus ARM demagnetization calculated for the 20–60 mT demagnetization interval. Linear correlation coefficients (r) are used to assess the definition of the slopes, and hence the quality of the RPI proxies. Several different RPI proxies were determined throughout the composite section at Site U1306, and the slopes of NRM/ARM were adopted as the optimal RPI proxy (Channell *et al.* 2014).

Although the 'Tensor' core orientation tool was used during IODP Expedition 303, the Site U1306 cores and other cores collected during the cruise could not be reliably or consistently oriented in azimuth (Expedition 303 Scientists 2006). For this reason, cores were oriented by rotating the mean component declination for each (∼10 m) core to north or south, depending on component inclination. This procedure is less problematic when several adjacent core sections from the same core are used, and becomes more uncertain for single core sections.

4 RESULTS

The CMS interval is represented in the composite section by the archive halves of core sections U1306C-18H-2 to 6 and core sections U1306A-19H-4 and 5. At this depth, the composite section tie between Hole U1306C and Hole U1306A is in core sections U1306C-18H-6 (138.9 cm) and U1306A-19H-4 (50.2 cm) at 180.32 mcd. We were permitted to sample entire core sections containing tie points in the composite section; therefore, magnetic measurements for these core sections extend beyond the tie point at each hole. In addition to core sections within the composite splice, we sampled and measured the working halves of core sections U1306A-19H-3 to 6, U1306B-19H-1 to 4, U1306C-18H-5 to 7 and U1306D-18H-4 to 6.

For each hole apart from one (Hole U1306D), we adopted the composite depths determined shipboard based on core scanning data such as magnetic susceptibility and reflectance (Expedition 303 Scientists 2006). For Hole U1306D, it was necessary to shift composite depths downsection by 1.8 m in order to obtain an acceptable match of CMS magnetization directions among the holes, implying an error of this magnitude in the composite depths at this level of Hole U1306D. Note that shipboard determinations of composite depth (mcd) do not account for relative stretching or compaction between holes (Expeditions 303 Scientists 2006), and therefore a uniform adjustment in mcd is unlikely to produce fully satisfactory hole-to-hole correlation.

Component magnetization directions at Site U1306 indicate that the CMS is manifested over about 5 m of core (Fig. 2), implying enhanced resolution relative to Sites 983/984 where the CMS is manifested over 2–3 m. As stated above, component magnetizations were calculated for a uniform (20–80 mT) peak field demagnetization interval. MAD values are generally below 10°, and often below 5° (Fig. 2), indicating that magnetization components are often well defined. Imperfect alignment of component magnetization in depth among holes (Fig. 2) is attributable to centimetre-scale inaccuracies in hole-to-hole correlations and the determination of composite depths, although variable lock-in depths of detrital remanent magnetization could be a contributing factor. Large swings in component declination are often not well correlated from hole to hole, implying that changes in field direction are not adequately captured at these sedimentation rates, and declination misalignments could be attributed to core orientation inaccuracies. Nonetheless, component magnetizations are moderately consistent from hole to hole (Fig. 2).

Examples of orthogonal projections of AF demagnetization of u-channels at specific depths (cm) in the working halves of core sections U1306D-18H-5 and U1306D-18H-6, from intervals with variable MAD values, at depths of 178.9–179.7 and 180.4–181.2 mcd (black dots in Fig. 2) are displayed in Figs S1 and S2 in the Supporting Information. Comparison of orthogonal projections from working and archive halves of core sections U1306A-19H-4 and U1306A-19H-5 from the 180.9–181.2 and 182.3–182.6 mcd intervals (orange and red dots for archive and working halves, respectively, in Fig. 2) are displayed in Figs S3 and S4 in the

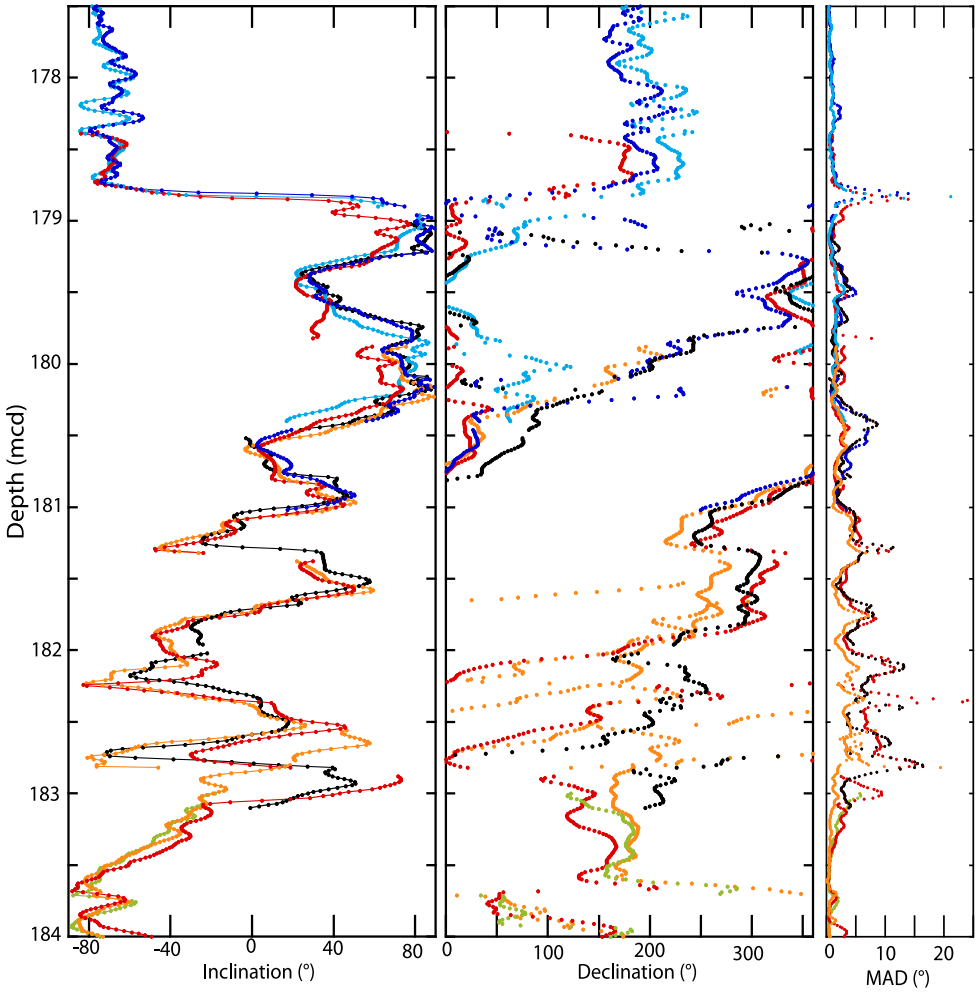

Figure 2. Cobb Mountain Subchron: Site U1306 component magnetization directions from the archive halves of Hole U1306A (orange) and Hole U1306C (light blue), and the working halves of Hole U1306A (red), U1306B (green), U1306C (dark blue) and U1306D (black). Component magnetizations determined for a uniform 20–80 mT demagnetization interval. MAD = maximum angular deviation.

Supporting Information. These intervals were chosen to display orthogonal projections where MAD values reach up to 15°, close to the maximum MAD values observed (Fig. 2). Orthogonal projections are labeled using the depth in core section (cm), depth in composite section (mcd) and the MAD value associated with the magnetization component determined for 20–80 mT peak demagnetization fields. Observation of orthogonal projections indicates that, in most cases, only minor changes in component magnetization direction would result from choosing a demagnetization interval other than 20–80 mT, and this led us to adopt a uniform demagnetization interval for calculation of component magnetization directions. Another observation from the orthogonal projections is the occasional presence of a high-coercivity, steep-down directed, magnetization component not demagnetized in peak fields of 80 mT. Because of the occasional presence of this high-coercivity component, possibly associated with drill-string magnetization/disturbance at these northerly site latitudes, we determine the magnetization components without anchoring to the origin of orthogonal projections.

The Site U1306 component magnetization directions (Fig. 2) are represented in Fig. 3 as VGP latitudes and are compared with the RPI proxies. Linear correlation coefficients (r) are used to ascertain the quality of the RPI proxies, and are close to unity other than for the older part of the RPI record from Hole U1306D where the slopes are poorly defined (Fig. 3). The shaded interval in Fig. 3 corresponds to the initial phases (1–2) of variable magnetization directions, discussed below.

The Site U1306 age model, back to 1.5 Ma, is based on a combination of oxygen isotope (δ^{18}O) data and RPI, although the δ^{18}O record does not extend beyond 1 Ma (Channell *et al.* 2014). Applying this RPI-based age model implies the onset of the CMS at ∼1215 ka, and the end at 1178 ka, leading to a duration of 37 kyr. The onset of the CMS is, however, recorded by very erratic magnetization directions and is more poorly defined than its termination. The RPI-based age model (Channell *et al.* 2014) implies that the CMS bridges the MIS 35–36 interval (Fig. 3). The RPI proxies decline in the 1215–1220 ka interval, and remain at low values during poorly resolved fluctuations in VGP latitude until ∼1194 ka. RPI proxies then increase as VGP latitudes exceed 40°N at ∼1190 ka (Fig. 3). The abrupt N–R transition in VGP latitude, which represents the end of the CMS, coincides with a RPI minimum at 1178 ka after which RPI proxies progressively increase (Fig. 3).

5 DISCUSSION

IODP Site U1308 in the central Atlantic Ocean (reoccupation of DSDP Site 609) has a continuous benthic δ^{18}O record that extends

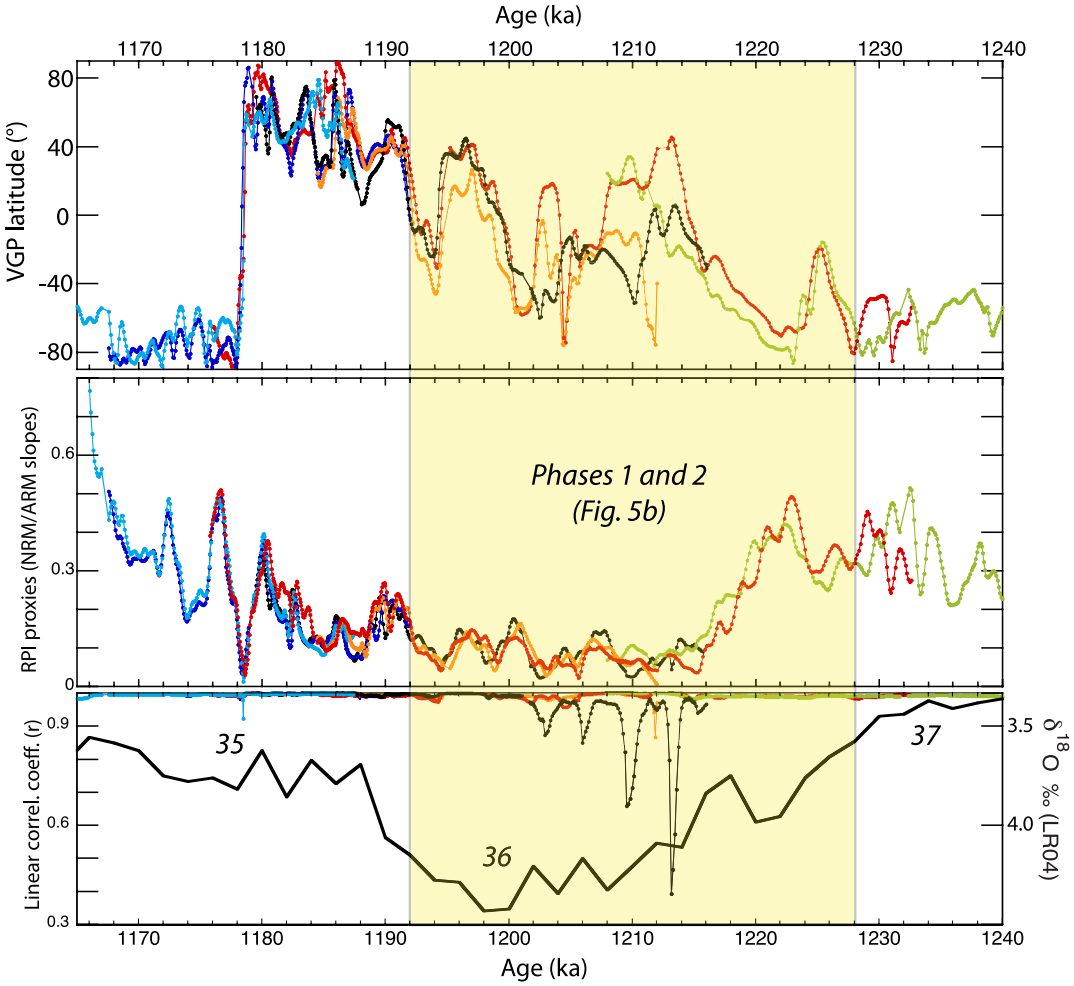

Figure 3. Cobb Mountain Subchron (CMS): Site U1306 virtual geomagnetic pole (VGP) latitudes determined from data in Fig. 2, relative palaeointensity (RPI) proxies (NRM/ARM slopes), linear correlation coefficients (r) associated with NRM/ARM slopes and the LR04 (Lisiecki & Raymo 2005) oxygen isotope template with marine isotope stages 35–37 labeled. Colour code as in Fig. 2. The shaded interval corresponds to VGPs during the initial phases of the CMS depicted in Fig. 5(b). Age model from Channell *et al*. (2014).

back into the Gauss Chron and provides a record of the CMS (Channell *et al.* 2008, 2016). The CMS at Site U1308 spans MIS 35–36 (Fig. 4), consistent with Site U1306 (Fig. 3). The Site U1308 CMS spans ∼1.4 m of sediment section and, therefore, the record has lower resolution than the CMS record at Site U1306 where it spans ∼5 m of section (Fig. 2). The component magnetizations at Site U1308 yield VGPs that pass northward through the Atlantic Ocean and then southward through the Pacific Ocean (Fig. 4). The VGPs associated with the CMS at Site U1306 are different and more complex (Fig. 5). The VGP path comprises several phases beginning with loops over the Indian Ocean (Phase 1, Fig. 5b), a return to high southern latitudes, looping as VGPs track northward through the Pacific Ocean (Phase 2), then proceed to high northern latitudes particularly in the NW Pacific (Phase 3) and North Atlantic (Phase 4) followed by an abrupt return through Africa to high southern latitudes (Phase 5). This highly complex directional behaviour is only broadly replicated among the holes at Site U1306 (Fig. 5). Discrepancies can be attributed to rapid changes in magnetization directions that are not adequately captured at these sedimentation rates, hole-to-hole variability in sedimentation and bioturbation, and perhaps unrecognized drilling and sampling disturbance. For example, it is often difficult to recognize drilling-related core twisting, compaction and stretching.

As mentioned above, ODP Sites 983 and 984 provided two of the higher resolution records of the CMS, where it is observed over 2–3 m of section. The Site 983/984 VGPs associated with the CMS (Fig. 6) yield a similar sequence of phases (1–5) to those observed at Site U1306 (Fig. 5). Looping over the Indian Ocean is followed by a VGP transit northward through the Pacific, and then through NW Pacific and North Atlantic VGPs, and finally an abrupt N–S VGP transit through Africa (Fig. 6). For both Site U1306 (Figs 3 and 5) and Sites 983/984 (Figs 1 and 6), the initial VGP loops over the Indian Ocean coincide with low RPI values, and RPI proxies increase as the VGPs transit northward through the Pacific Ocean. The shaded interval in Fig. 3 corresponds to initial phases (1–2) of the CMS depicted in Fig. 5(b). According to Channell *et al.* (2009), the CMS is associated with the lowest RPI values in the last 1.5 Myr.

6 CONCLUSIONS

The CMS at Site U1306 is correlated to the MIS 35–36 interval and has an apparent duration of 37 kyr from 1178 to 1215 ka

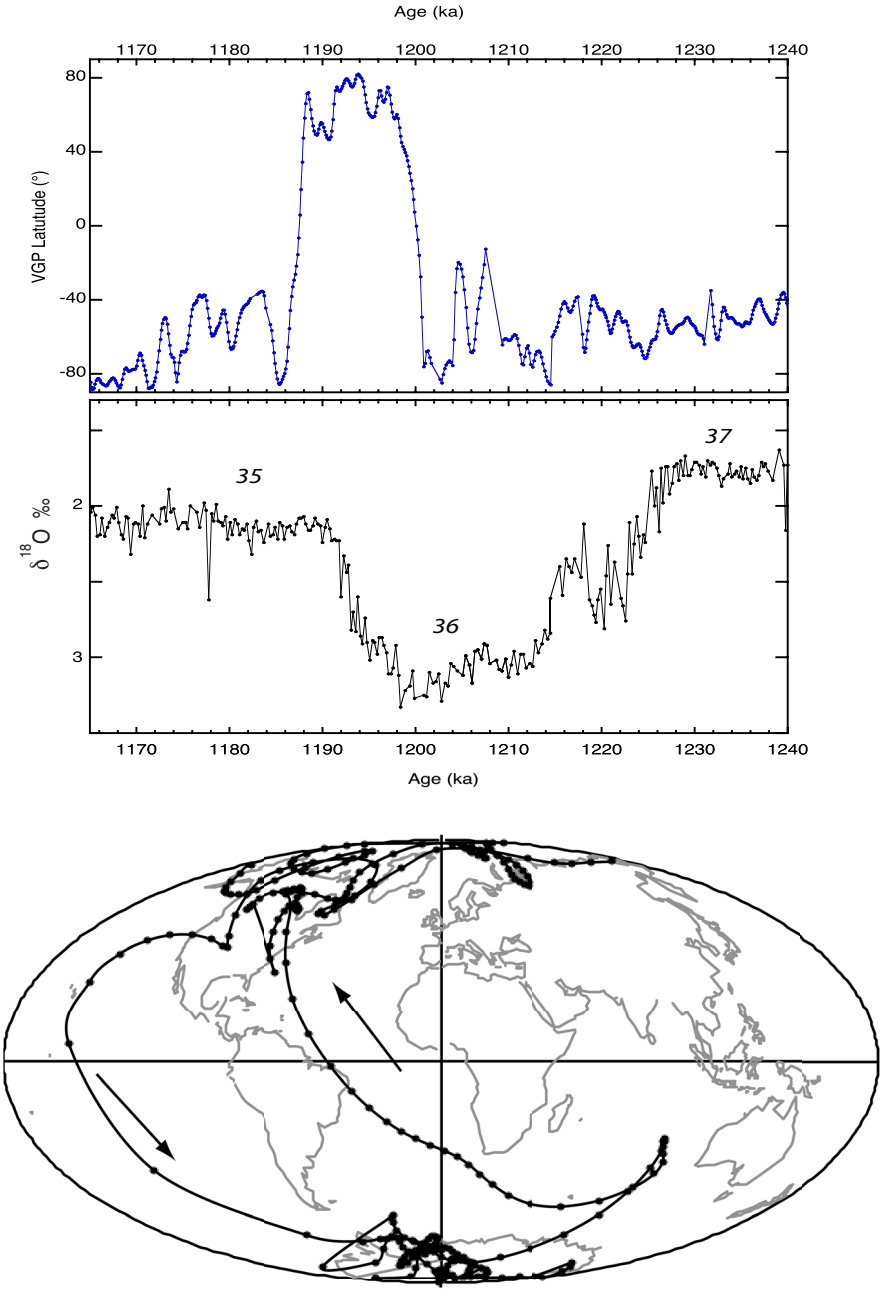

Figure 4. Cobb Mountain Subchron: Site U1308 virtual geomagnetic pole (VGP) latitudes and benthic oxygen isotope data, with marine isotope stages 35–37 labeled, and VGPs on a global projection (data from Channell *et al.* 2008, 2016).

(Fig. 3), although the onset of the CMS is poorly defined by erratic magnetization directions that are not well correlated from hole-to-hole (Fig. 2) at a time when RPI apparently reached low values (Fig. 3). Some correlation misfits could be attributed to errors in depth (mcd) and in hole-to-hole correlations, centimetre-scale variations in deposition among holes at the site, and possibly unrecognized drilling and sampling disturbance.

Over 15 yr ago, CMS records were used to infer large-scale dipolar geomagnetic field symmetries throughout the CMS (Clement 1992, 2000; Yang *et al.* 2001). VGP paths for the CMS at Site U1306 (Fig. 5) are more complex than the VGP path from Site U1308 (Fig. 4), and VGP paths from DSDP Site 609 and other sites that record the CMS (e.g. Hsu *et al.* 1990; Clement & Martinson 1992; Abrahamsen & Sager 1994). On the other hand, the higher resolution CMS records (Clement 2000; Yang *et al.* 2001) indicate initial VGP loops over the Indian Ocean, followed by an R–N transition through the Pacific Ocean and a final N–R transition through Africa. This VGP pattern broadly corresponds to VGP transits observed at Site U1306.

Differences between previously published VGP paths during the CMS and the Site U1306 records indicate that VGP paths are variably smoothed renditions of the geomagnetic field during this brief

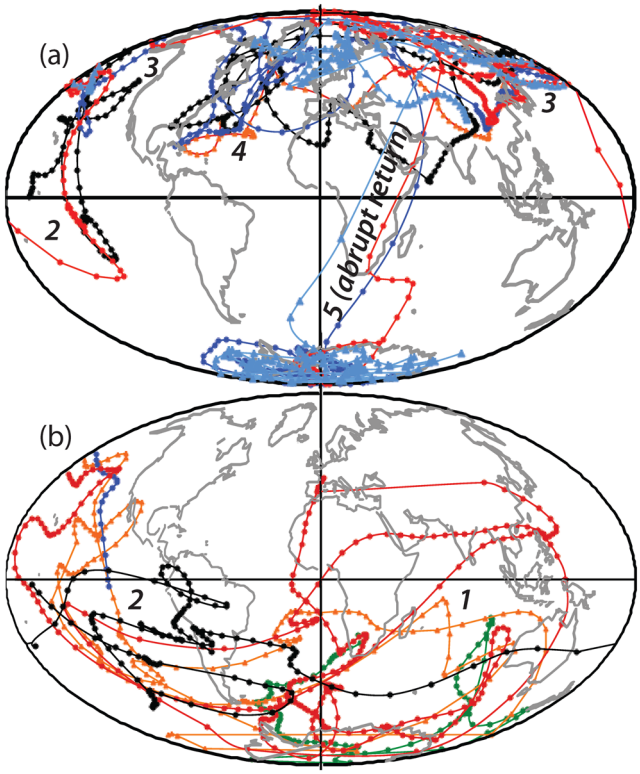

Figure 5. Cobb Mountain Subchron (CMS): Site U1306 virtual geomagnetic poles (VGPs) corresponding to the directional data in Fig. 2, using the same colour code. (a) Later phases of the CMS from 177.5 to 181.0 metres composite depth (mcd). (b) Earlier phases of the CMS from 181.0 to 184.0 mcd. Depths of 181.0 and 184.0 mcd correspond to 1192 and 1228 ka, respectively. Numbers on VGP paths refer to phases discussed in the text.

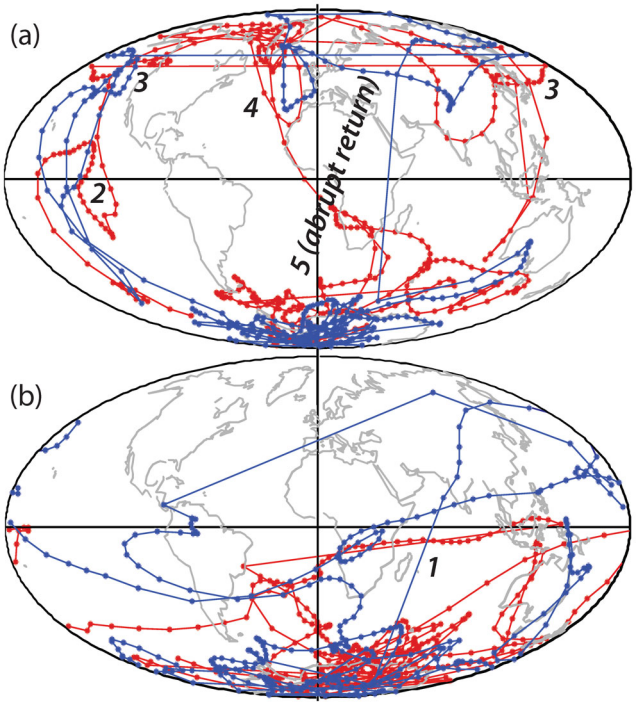

Figure 6. Cobb Mountain Subchron (CMS): ODP Site 983 (red) and Site 984 (blue) virtual geomagnetic poles (VGPs) corresponding to the directional data in Fig. 1 (from Channell *et al.* 2002). (a) Later phases of the CMS above 150.4 metres composite depth (mcd) at Site 983, and 153.6 mcd at Site 984. (b) Earlier phases of the CMS below 150.4 mcd at Site 983, and 153.6 mcd at Site 984. Depths of 150.4 mcd at Site 983 and 153.6 mcd at Site 984 correspond to 1204 and 1207 ka, respectively. Age model from Channell *et al*. (2002). Numbers on VGP paths refer to phases discussed in the text.

polarity subchron. It is worth noting that smoothing the higher sedimentation rate records, by a simple function proportional to sedimentation rate difference, do not yield similarity with the lower sedimentation rate records.

The Site U1306 CMS VGP paths (Fig. 5) can be loosely matched to the CMS VGPs from ODP Sites 983/984 (Fig. 6). The Site U1306 CMS record is likely to be a more faithful rendition of the geomagnetic field during the CMS than the lower resolution CMS records such as those from Site U1308 (DSDP Site 609) and from the western Pacific Ocean (Hsu *et al.* 1990; Abrahamsen & Sager 1994). At Site U1306, poorly replicated initial VGP loops centred on the Indian Ocean are followed by a complex northerly transit through the Pacific Ocean, relative stasis at high northern latitudes particularly in the NW Pacific and North Atlantic, and an abrupt transit to southern latitudes through Africa (Fig. 5).

Rather than advocating for dipole field symmetry during the CMS (e.g. Clement 2000), we speculate that broad similarities among CMS VGP paths may be attributed to regions of increased vertical field intensity in the North Atlantic and NW Pacific, analogous to flux patches in the top-core field beneath North America and NE Asia that appear in the time-averaged historical field, and perhaps also in the longer term time-averaged field (e.g. Kelly & Gubbins 1997; Gubbins *et al.* 2006; Amit *et al.* 2011; Constable & Korte 2015). Similarly located flux patches may have dominated during the demise of the axial dipole field at the time of the CMS. RPI values are particularly low during the initial phase of the CMS (Fig. 3) that corresponds to erratic VGP loops over the Indian Ocean (Fig. 5b). These loops may be an expression of multiple rapid transits of the VGP between high southern latitudes and the NW Pacific flux patch. The VGP path becomes better defined as RPI values increase in the middle part of the CMS, with VGP clusters in North America and the NW Pacific, before an abrupt RPI minimum coincides with the abrupt N–S directional change that marks the end of the CMS (Fig. 3).

ACKNOWLEDGEMENTS

This research was supported by the US National Science Foundation grants EAR-1014506 and OCE-0850413. I thank Alain Mazaud, Joe Stoner and Helen Evans for assistance with the initial phase of sampling, and Kainian Huang for work in the palaeomagnetic laboratory. The manuscript benefitted from a characteristically careful review by Andy Roberts, and the editorial comments of Richard Holme. I also acknowledge the support of the curatorial staff at the IODP core repository in Bremen, and the Captain, crew, technical staff and shipboard scientists during IODP Expedition 303. Data are archived at the Pangaea Database (www.pangaea.de).

REFERENCES

Abrahamsen, N. & Sager, W., 1994. Cobb Mountain geomagnetic polarity event and transitions in three deep-sea sediment cores from the Lau Basin, in *Proceedings of ODP Scientific Results*, Vol. 135, pp. 737–762, eds Hawkins, J. *et al.*, Ocean Drilling Program, College Station, TX.

Amit, H., Korte, M., Aubert, J., Constable, C. & Hulot, G., 2011. The time-dependence of intense archeomagnetic flux patches, *J. geophys. Res.,* **116,** B12106, doi:10.1029/201JB008538.

Channell, J.E.T. & Raymo, M.E., 2003. Paleomagnetic record at ODP Site 980 (Feni Drift, Rockall) for the past 1.2 Myrs, *Geochem. Geophys. Geosyst.,* **4,** doi:10.1029/2002GC000440.

Channell, J.E.T. & Guyodo, Y., 2004. The Matuyama Chronozone at ODP Site 982 (Rockall Bank): evidence for decimeter-scale magnetization lock-in depths, in *Timescales of the Geomagnetic Field,* AGU Geophys. Monogr. Ser., Vol. 145, pp. 205–219, eds Channell, J.E.T. *et al.*, American Geophysical Union.

Channell, J.E.T., Mazaud, A., Sullivan, P., Turner, S. & Raymo, M.E., 2002. Geomagnetic excursions and paleointensities in the 0.9–2.15 Ma interval of the Matuyama Chron at ODP Site 983 and 984 (Iceland Basin), *J. geophys. Res.,* **107**(B6), doi:10.1029/2001JB000491.

Channell, J.E.T., Hodell, D.A., Xuan, C., Mazaud, A. & Stoner, J.S., 2008. Age calibrated relative paleointensity for the last 1.5 Myr at IODP Site U1308 (North Atlantic), *Earth planet. Sci. Lett.,* **274,** 59–71.

Channell, J.E.T., Xuan, C. & Hodell, D.A., 2009. Stacking paleointensity and oxygen isotope data for the last 1.5 Myrs (PISO-1500), *Earth planet. Sci. Lett.,* **283,** 14–23.

Channell, J.E.T., Wright, J.D., Mazaud, A. & Stoner, J.S., 2014. Age through tandem correlation of Quaternary relative paleointensity (RPI) and oxygen isotope data at IODP Site U1306 (Eirik Drift, SW Greenland), *Quat. Sci. Rev.,* **88,** 135–146.

Channell, J.E.T., Hodell, D.A. & Curtis, J.H., 2016. Relative paleointensity (RPI) and oxygen isotope stratigraphy at IODP Site U1308: North Atlantic RPI stackfor 1.2–2.2 Ma (NARPI-2200) and age of the Olduvai Subchron, *Quat. Sci. Rev.,* **131,** 1–19.

Clement, B.M., 1992. Evidence for dipolar fields during the Cobb Mountain geomagnetic polarity reversals, *Nature,* **358,** 405–407.

Clement, B.M., 2000. Comment on the Lau Basin Cobb Mountain records by Abrahamsen and Sager, *Phys. Earth planet. Inter.,* **119,** 173–184.

Clement, B.M. & Kent, D.V., 1987. Short polarity intervals within the Matuyama: transition field records from hydraulic piston cored sediments from the North Atlantic, *Earth planet. Sci. Lett.,* **81,** 253–264.

Clement, B.M. & Martinson, D.G., 1992. A quantitative comparison of two paleomagnetic records of the Cobb Mountain subchron from North Atlantic deep-sea sediments, *J. geophys. Res.,* **97,** 1735–1752.

Constable, C. & Korte, M., 2015. Centennial- to millennial-scale geomagnetic field variations, in *Treatise on Geophysics: Geomagnetism,* Vol. 5, Chapter 9, pp. 309–341, ed. Kono, M., Elsevier, Amsterdam.

Expedition 303 Scientists, 2006. Site U1306, in *Proceedings of IODP Expedition 303/306 Scientists*, Vol. 303, eds Channell, J.E.T., Kanamatsu, T., Sato, T., Stein, R., Alvarez Zarikian, C.A. & Malone, M.J., Integrated Ocean Drilling Program Management International, Inc., College Station, TX, doi:10.2204/iodp.proc.303306.103.

Gubbins, D., Jones, A.L. & Finlay, C.C., 2006. Fall in Earth's magnetic field is erratic, *Science,* **312,** 900–902.

Guyodo, Y., Richter, C. & Valet, J-P., 1999. Paleointensity record from Pleistocene sediments (1.4-0 Ma) off the California Margin, *J. geophys. Res.,* **104,** 22 953–22 964.

Guyodo, Y., Acton, G.D., Brachfeld, S. & Channell, J.E.T., 2001. A sedimentary paleomagnetic record of the Matuyamachron from the western Antarctic margin, *Earth planet. Sci. Lett.,* **191,** 61–74.

Guyodo, Y., Channell, J.E.T. & Thomas, R., 2002. Deconvolution of u-channel paleomagnetic data near geomagnetic reversals and short events, *Geophys. Res. Lett.,* **29,** 1845, doi:10.1029/2002GL014963.

Hayashida, A., Verosub, K.L., Heider, F. & Leonhardt, R., 1999. Magnetostratigraphy and relative paleointensity of late Neogene sediments at ODP Leg 167 Site 1010 off Baja California, *Geophys. J. Int*., **139,** 829–840.

Horng, C.S., Lee, M.Y., Pälike, H., Wei, K-Y., Liang, W.T., Iizuka, Y. & Torii, M., 2002. Astronomically calibrated ages for geomagnetic reversals within the Matuyama Chron, *Earth Planets Space,* **54,** 679–690.

Horng, C.S., Roberts, A.P. & Liang, W.T., 2003. A 2.14-Myr astronomically tuned record of relative geomagnetic paleointensity from the western Philippine Sea, *J. geophys. Res.,* **108,** 2059, doi:10.1029/2001JB001698.

Hsu, V., Merrill, D.L. & Shibuya, H., 1990. Paleomagnetic transition records of the Cobb Mountain Event from sediments of the Celebes and Sulu Seas, *Geophys. Res. Lett.,* **17**(11), 2069–2072.

Kawamura, N., Ishikawa, N. & Torii, M., 2012. Diagenetic alteration of magnetic minerals in Labrador Sea sediments (IODP Sites U1305, U1306, and U1307), *Geochem., Geophys., Geosyst.,* **13,** Q08013, doi:10.1029/2012GC004213.

Kelly, P. & Gubbins, D., 1997. The geomagnetic field over the past 5 million years, *Geophys. J. Int.,* **128,** 315–330.

Kirschvink, J.L., 1980. The least squares lines and plane analysis of paleomagnetic data, *Geophys. J. R. astr. Soc.,* **62,** 699–718.

Kuiper, K.F., Deino, A., Hilgen, F.J., Krijgsman, W., Renne, P.F. & Wijbrans, J.R., 2008. Synchronizing rock clocks of Earth history, *Science,* **320,** 500–504.

Lisiecki, L. E. & Raymo, M.E., 2005. A Pliocene-Pleistocene stack of 57 globally distributed benthic δ^{18}O records, *Paleoceanography,* **20,** PA1003, doi:10.1029/2004PA001071.

Mankinen, E.A. & Grommé, C.S., 1982. Paleomagnetic data from the Cosa Range, California, and current status of the Cobb Mountain normal geomagnetic polarity event, *Geophys. Res. Lett.,* **9,** 1239–1282.

Mankinen, E.A., Donnelly, J.M. & Grommé, C.S., 1978. Geomagnetic polarity event recorded at 1.1 m.y.b.p. on Cobb Mountain, Clear Lake volcanic field, California, *Geology,* **6,** 653–656.

Nomande, S., Renne, P.R., Vogel, N., Deino, A.L., Sharp, W.D., Becker, T.A., Jaouni, A.R. & Mundil, R., 2005. Alder Creek sanidine (ACs-2): a Quaternary ^{40}Ar/^{39}Ar dating standard tied to the Cobb Mountain geomagnetic event, *Chem. Geol*., **218,** 315–338.

Panaiotu, C.G., Jicha, B.R., Singer, B.S., Tugui, A., Seghedi, I., Panaiotu, A.G. & Necula, C., 2013. ^{40}Ar/^{39}Ar chronology and paleomagnetism of Quaternary basaltic lavas from the Persani Mountains (East Carpathians), *Phys. Earth planet. Inter.,* **221,** 1–14.

Raymo, M.E., Ganley, K., Carter, S., Oppo, D.W. & McManus, J., 1998. Millennial-scale climate instability during the early Pleistocene epoch, *Nature,* **392,** 699–702.

Ruddiman, W.F., Raymo, M.E., Martinson, D.G., Clement, B.M. & Backman, J., 1989. Pleistocene evolution: northern hemisphere ice sheet and north Atlantic ocean, *Paleoceanography,* **4,** 353–412.

Shackleton, N.J., Berger, A. & Peltier, W.R., 1990. An alternative astronomical calibration of the lower Pleistocene timescale based on ODP Site 677, *Trans. R. Soc. Edinb.: Earth Sci.,* **81,** 251–261.

Singer, B.S., 2014. A Quaternary geomagnetic instability time scale, *Quat. Geochron*., **21,** 29–52.

Turrin, B.D., Donnelly-Nolan, J.M. & Hearn, B.C., Jr., 1994. ^{40}Ar/^{39}Ar ages from the rhyolite of Alder Creek, California: age of the Cobb Mountain normal polarity subchron revisited, *Geology,* **22,** 251–254.

Weeks, R., Laj, C., Endignoux, L., Fuller, M., Roberts, A.P., Manganne, R., Blanchard, E. & Goree, W., 1993. Improvements in long-core measurement techniques: applications in palaeomagnetism and palaeoceanography, *Geophys. J. Int.,* **114,** 651–662.

Xuan, C. & Channell, J.E.T., 2009. UPmag: MATLAB software for viewing and processing u-channel or other pass-through paleomagnetic data, *Geochem. Geophys. Geosyst.,* **10,** Q10Y07, doi:1029/2009GC002584.

Xuan, C., Channell, J.E.T. & Hodell, D.A., 2016. Quaternary paleomagnetic and oxygen isotope records from diatom-rich sediments from the southern Gardar Drift (IODP Site U1304), *Quat. Sci. Rev.,* **142,** 74–89.

Yamazaki, T. & Oda, H., 2005. A geomagnetic paleointensity stack between 0.8 and 3.0 Ma from equatorial Pacific sediment cores, *Geochem. Geophys. Geosyst.,* **6**(11), doi:10.1029/2005GC001001.

Yang, Z., Clement, B.M., Acton, G.D., Lund, S.P., Okada, M. & Williams, T., 2001. Record of the Cobb Mountain Subchron from the Bermuda Rise (ODP Leg 172), *Earth planet Sci. Lett.,* **193,** 303–313.

SUPPORTING INFORMATION

Supplementary data are available at *GJIRAS* online.

Figure S1. Core section U1306D-18H-5 working half: orthogonal projections of alternating field demagnetization, for the 20–80 mT

peak field range, from u-channel data for specific depths (cm) in the core section and depths (mcd) in the sediment sequence (see the main-text Fig. 2). Blue and red symbols represent projection on the horizontal and vertical planes, respectively. Intensity scales $\times 10^{-2}$ A m^{-1}. All projections plotted with north and up towards the top of page. Declinations in orthogonal projections are not corrected for core orientation as in the main-text Fig. 2. Maximum angular deviation (MAD) values are given for magnetization components calculated in the 20–80 mT demagnetization range. Component magnetizations for U1306D-18H-5 are shown in the main-text Fig. 2 by black symbols.

Figure S2. Core section U1306D-18H-6 working half: orthogonal projections of alternating field demagnetization, for the 20–80 mT peak field range, from u-channel data for specific depths (cm) in the core sections and depths (mcd) in the sediment sequence (see the main-text Fig. 2). Blue and red symbols represent projection on the horizontal and vertical planes, respectively. Intensity scales $\times 10^{-2}$ A m^{-1}. All projections plotted with north and up towards the top of page. Declinations in orthogonal projections are not corrected for core orientation as in the main-text Fig. 2. Maximum angular deviation (MAD) values are given for magnetization components calculated in the 20–80 mT demagnetization range. Component magnetizations for U1306D-18H-6 are shown in the main-text Fig. 2 by black symbols.

Figure S3. Core section U1306A-19H-4, archive (top) and working halves (below): orthogonal projections of alternating field demagnetization, for the 20–80 mT peak field range, from u-channel data for specific depths (cm) in the core sections and depths (mcd) in the sediment sequence (see the main-text Fig. 2). Blue and red symbols represent projection on the horizontal and vertical planes, respectively. Intensity scales $\times 10^{-2}$ A m^{-1}. All projections plotted with north and up towards the top of page. Declinations in orthogonal projections are not corrected for core orientation as in the main-text Fig. 2. Maximum angular deviation (MAD) values are given for magnetization components calculated in the 20–80 mT demagnetization range. Component magnetizations for U1306A-19H-4 are shown in the main-text Fig. 2 by orange and red symbols for archive and working halves, respectively.

Figure S4. Core section U1306A-19H-5, archive (top) and working halves (below): orthogonal projections of alternating field demagnetization, for the 20–80 mT peak field range, from u-channel data for specific depths (cm) in the core sections and depths (mcd) in the sediment sequence (see the main-text Fig. 2). Blue and red symbols represent projection on the horizontal and vertical planes, respectively. Intensity scales $\times 10^{-2}$ A m^{-1}. All projections plotted with north and up towards the top of page. Declinations in orthogonal projections are not corrected for core orientation as in the main-text Fig. 2. Maximum angular deviation (MAD) values are given for magnetization components calculated in the 20–80 mT demagnetization range. Component magnetizations for U1306A-19H-5 are shown in the main-text Fig. 2 by orange and red symbols for archive and working halves, respectively.